Atmospheric nitrogen deposition fluxes into coastal wetlands and their impacts on ecosystem carbon sequestration in East Asia

Jia Liu[1], Yan Zhang[1,2,3], Shenglan Jiang[1], Yuqi Xiong[1], Chenji Jin[1], Qi Yu[1], Weichun Ma[1]

[1]Shanghai Key Laboratory of Atmospheric Particle Pollution and Prevention, National Observations and Research Station for Wetland Ecosystems of the Yangtze Estuary, Department of Environmental Science and Engineering, Fudan University, Shanghai 200433, China

[2]MOE laboratory for National Development and Intelligent Governance, Shanghai institute for energy and carbon neutrality strategy, IRDR ICoE on Risk Interconnectivity and Governance on Weather/Climate Extremes Impact and Public Health, Fudan University, Shanghai 200433, China

[3] Shanghai Institute of Eco-Chongming (SIEC), Shanghai, 200062, China

Correspondence to: Yan Zhang (yan_zhang@fudan.edu.cn)

Abstract. Coastal wetlands serve as critical sinks for both carbon and nitrogen within regional ecosystems, playing an essential role in mitigating atmospheric greenhouse gases and nutrient enrichment. This study integrates high-resolution wetland type data, AIS-based ship emission inventories, and regional nitrogen deposition simulations to quantify nitrogen inputs to East Asian coastal wetlands from the perspective of source–sink coupling. Firstly, the atmospheric nitrogen deposition fluxes in coastal wetland areas of East Asia were simulated and evaluated with WRF-CMAQ. Nitrogen deposition fluxes were spatially coupled with classified wetland maps in ArcGIS. Net primary productivity (NPP) was estimated using a modified CASA light-use efficiency model, incorporating solar radiation and FPAR from remote sensing. Carbon sequestration and oxygen release were then quantified using stoichiometric relationships based on NPP. The results indicate that total nitrogen deposition across East Asian coastal wetlands follows a general gradient of "high in the south, low in the north" and "strong in urban-industrial clusters, weak in remote coastal zones." On average, ship emissions contribute 10.13 % and 15.22 % to NO_3^--N and NH_4^+-N deposition, respectively, while their contribution to gaseous NH_3-N is negligible. Among wetland types, salt marshes receive the highest nitrogen input per unit area (654.99 mg NO_3^--N·m^{-2}·yr^{-1}), although tidal flats dominate total regional nitrogen input due to their extensive spatial coverage. Dry and wet deposition exhibit significant seasonal variation: wet deposition consistently prevails during the spring and summer months due to frequent rainfall, while dry deposition becomes increasingly prominent in autumn and winter. For instance, in the Korean Peninsula, the wet-dry gap in nitrate deposition reaches 0.17 g N·m^{-2}·yr^{-1}, while the Yangtze River Delta exhibits relatively balanced ammonium inputs (dry-wet difference of only 0.05 g N·m^{-2}·yr^{-1}). Carbon sequestration capacity shows strong spatial and temporal coupling with nitrogen deposition. Mangrove forests exhibit the highest annual NPP (~776.16 g C·m^{-2}·yr^{-1} in summer), supported by high FPAR and solar radiation (1749.29 MJ·m^{-2}), followed by salt marshes and tidal flats. Seasonal patterns reveal a summer peak in carbon uptake across all wetland types, with mangrove NPP in summer being two times higher than winter values. Nitrogen deposition primarily enhances carbon sequestration during warm seasons; for instance, in the mangroves of the Pearl River Delta, nitrogen inputs increase summer CO_2 fixation by 6.85 g C·m^{-2}, while the effect is negligible in winter (<0.06 %) or in nitrogen-saturated regions. These findings provide a scientific foundation for understanding how coastal ecosystems respond to anthropogenic activities and long-range nitrogen transport. Furthermore, the results serve as an important reference for wetland conservation, nitrogen cycle management, and the development of regional carbon neutrality strategies.

1 Introduction

Coastal wetlands, functioning as dynamic interfaces between terrestrial and marine systems, serve not only as critical habitats for global biodiversity but also as integral components of regional and global ecosystems (Wang et al., 2025; Huang et al., 2025). In East Asia, these wetlands exhibit considerable heterogeneity, encompassing mangrove forests, salt marshes, mudflats, coral reefs, and seagrass beds—each characterized by distinct ecological functions. Mangrove forests mitigate storm surges through their complex root systems and play a vital role in carbon sequestration. Globally mangrove habitats stocked an

average of 693 t C_{org} ha^{-1}, which is 15–24 % of the tropical coastal ocean carbon burial rate of 184 g C_{org} m^{-2} yr^{-1} (Rani et al., 2023). Salt marshes, with salt-tolerant vegetation, can retain heavy metals and organic pollutants in response to tidal dynamics. Mudflats mitigate flood and tidal impacts by facilitating sediment deposition. Coral reefs and seagrass beds sustain marine

45 biodiversity through biocalcification and primary production. In recent decades, however, coastal wetlands have faced increasing threats from land reclamation, industrial and agricultural pollution, and climate change. Consequently, their areal extent has declined by approximately 35 %, according to regional remote sensing data, and the degradation of their ecological functions poses serious challenges to the global carbon cycle and coastal zone stability (Barbier et al., 2011; Goldberg et al., 2020; Li et al., 2018).

50 Against this backdrop, nitrogen deposition, resulting from anthropogenic emissions and atmospheric chemical processes (Gruber and Galloway, 2008), has emerged as a key driver reshaping the ecological dynamics of coastal wetlands. Acting as a "double-edged sword," atmospheric nitrogen—delivered via dry and wet deposition—directly influences NPP and carbon sequestration potential. Nitrogen and carbon cycles are inherently interconnected (Cheng et al., 2018). Previous studies have shown that moderate nitrogen inputs (<10 kg N ha^{-1} yr^{-1} can stimulate photosynthetic activity in mangrove and salt marsh

55 vegetation, enhance biomass accumulation, and promote the storage of soil organic carbon (Rong and Rui-Ying, 2015; Adam Langley et al., 2013; Morris and Bradley, 1999). However, rapid industrialization and agricultural intensification across East Asia have led to nitrogen deposition levels exceeding 20 kg N ha^{-1} yr^{-1} in some regions, such as the Yangtze River Delta (YRD). This excessive nitrogen may induce an imbalance in the nitrogen-to-phosphorus ratio, potentially triggering cascading ecological effects (Liu et al., 2013). On one hand, excessive nitrogen promotes microbial heterotrophic respiration, accelerating

60 the mineralization of soil organic matter and potentially transforming wetlands from carbon sinks into carbon sources. On the other hand, intensified nitrification–denitrification processes may increase the emission of greenhouse gases such as N_2O and disrupt symbiotic relationships between benthic fauna and plant communities, potentially leading to biodiversity loss. Moreover, the ecological impacts of nitrogen deposition are spatially heterogeneous: mangrove forests may retain nitrogen due to their anaerobic root environments, while unvegetated mudflats may facilitate nitrogen migration via surface runoff,

65 increasing the risk of eutrophication in adjacent marine waters (Sasmito et al., 2020). Therefore, quantifying nitrogen deposition fluxes and their spatiotemporal distribution is critical for understanding the atmospheric nitrogen inputs into coastal wetland ecosystems. A comprehensive understanding of both the intensity and variability of nitrogen input is essential for enhancing carbon sequestration, optimizing nutrient regulation, and supporting the achievement of regional carbon neutrality targets.

70 Coastal wetlands, in addition to their role as biodiversity hotspots, also function as critical regulators of the carbon–nitrogen–phosphorus (C–N–P) cycles. However, multiple anthropogenic and climatic stressors—such as land reclamation, industrial and agricultural emissions, and sea-level rise—have led to a 40 % reduction in the total area of coastal wetlands in East Asia in recent decades (Yoshikai et al., 2021; Li et al., 2020; Leidner and Buchanan, 2018), substantially weakening their ecological functions and threatening the stability of the global carbon cycle and coastal systems.

75 In the international context, nitrogen deposition has become a focal issue in global change ecology, particularly concerning its ecological impacts on coastal wetlands. Long-term studies in Europe and North America have explored nitrogen input mechanisms across various wetland types. For instance, observations in the salt marshes of Chesapeake Bay, USA, have demonstrated that atmospheric nitrogen deposition can significantly alter the soil nitrogen-to-phosphorus ratio (N:P > 16), thereby suppressing reed root development and reducing wetland carbon sequestration efficiency by 12 %–18 % (Deegan et

80 al., 2012; Morris, 1991). Research along the North Sea coast further shows that nitrogen deposition, in conjunction with tidal hydrodynamics, accelerates the mineralization of sedimentary organic nitrogen and enhances N_2O emissions via nitrification, contributing approximately 7 %–9 % to regional greenhouse gas budgets (Marchant et al., 2018; Barnes and Upstill-Goddard, 2011; Bange, 2006). In tropical mangrove systems, studies from Southeast Asia reveal that excessive nitrogen deposition (>25 kg N ha^{-1} yr^{-1}) inhibits symbiotic nitrogen-fixing bacteria and facilitates the invasion of non-native species such as Spartina

85 alterniflora, ultimately destabilizing native ecosystems (Xia et al., 2021; Chakraborty, 2019; Porter et al., 2013). However, these studies often focus on individual wetland types within specific climate zones and lack integrative, cross-scale assessments of nitrogen deposition dynamics in the ecologically diverse coastal wetlands of East Asia.

Recent domestic research has advanced our understanding of this issue. Field observations in the salt marshes of the YRD

indicate that ammonium nitrogen (NH_4^+) from industrial emissions accounts for approximately 65 % of total atmospheric

90 nitrogen deposition in the region(Xu et al., 2018b). While such nitrogen input temporarily enhances carbon sequestration by promoting the biomass of Suaeda salsa (Hong et al., 2024; Chen and Sun, 2020), long-term deposition leads to soil acidification (pH decline of 0.3–0.5) and increased mobility of heavy metals, such as a 40 % rise in cadmium activity (Hu et al., 2019). Modelling studies by Wu et al. further show that during the first two decades of elevated nitrogen deposition, plant productivity, autotrophic respiration, and litter production increase sharply, resulting in significant alterations to ecosystem carbon fluxes.

95 Beyond this initial phase, carbon cycling becomes constrained primarily by vegetation composition and biomass distribution within the newly stabilized ecosystem (Wu et al., 2015). In the mudflats of Bohai Bay, where vegetation cover is minimal, studies suggest that 30 %–50 % of deposited nitrogen is transported into adjacent marine environments via surface runoff, contributing significantly to the eutrophication of the Yellow Sea (Fu et al., 2021; Zheng and Zhai, 2021). Despite these insights, existing research remains largely limited to single environmental media, specific wetland types, or short temporal

100 scales. There is a pressing need for systematic, regionally comparative assessments of nitrogen deposition patterns and their ecological consequences across multiple wetland categories in East Asia.

In view of the significant disparities that exist among various coastal wetland types, their carbon and nitrogen fixation pathways, efficiencies, and ecosystem responses are influenced by multiple factors, including vegetation characteristics, soil properties, hydrodynamics, and nitrogen input intensity (Fettrow et al., 2024; Alongi, 2020). Given the dual roles of coastal wetlands as

105 carbon and nitrogen sinks, their functions have attracted increasing attention in the context of climate change mitigation and regional environmental governance. Nevertheless, a comprehensive understanding of nitrogen deposition fluxes, spatiotemporal variability, and their regulatory influence on carbon sequestration processes remains incomplete. To address this gap, the present study focuses on six representative coastal wetland systems in East Asia—specifically mangrove forests, salt marshes, and tidal flats. The objectives are to (1) examine the seasonal and regional variation of nitrogen deposition fluxes

110 under different climatic conditions and vegetation types; (2) quantify their impacts on NPP and CO_2 fixation; and (3) analyse the coupling mechanisms between nitrogen deposition and carbon sink capacity. This research aims to elucidate key ecological processes and spatial heterogeneity in the synergistic regulation of carbon and nitrogen cycles in coastal wetlands. The findings are expected to support improved assessments of ecosystem services, inform nitrogen pollution control policies, and contribute to wetland conservation strategies aligned with regional carbon neutrality goals.

115   2 Materials and Methods

The East Asia region is located in the eastern part of Asia, bordering the Pacific Ocean to the east. It encompasses countries and regions such as China, Japan, South Korea, and North Korea, featuring diverse geographical environments and rich ecosystems. This region is not only one of the most dynamic areas in global economic development, but also boasts a coastal wetland system of great ecological value. Coastal wetlands in East Asia are widely distributed along the eastern coast of China,

120 the west coast of the Korean Peninsula (KP) and the coast of the Japanese archipelago. They mainly include types such as salt marshes, mudflats, mangrove forests and estuarine deltas. These wetlands play an irreplaceable ecological role in maintaining biodiversity, resisting storm surges, and purifying water quality.

2.1 Emission and Land Cover in East Asia

This study focuses on the East Asian region, including mainland China and neighbouring countries. For mainland China, the

125 2017 Multi-resolution Emission Inventory for China (MEIC) (Zheng et al., 2018; Li et al., 2017a) was used as the anthropogenic emissions dataset. For other regions of East Asia, the 2010 MIX Asian emissions inventory was employed (Li et al., 2017b). The ship-based emission inventory for conventional atmospheric pollutants was constructed using a bottom-up approach based on real-time data from the 2017 Automatic Identification System (AIS). This method calculates emissions using fuel consumption-based emission factors specific to different marine fuels and adjusts for individual vessel

130 characteristics, such as engine type and operational status (Yuan et al., 2023; Fan et al., 2016). The resulting ship emissions inventory includes nitrogen oxides (NO_x), ammonia (NH_3), and particulate matter ($PM_{2.5}$, PM_{10}). Detailed computational procedures are provided in Supplementary Section 1.1. Emission factors used for these species are listed in Supplementary

Table S1, with units expressed in grams per kilowatt-hour (g (kWh)$^{-1}$).

AI Earth (https://engine-aiearth.aliyun.com) is a cloud-based geospatial platform that provides a wide range of environmental
135   datasets, including meteorological, land surface, and atmospheric composition variables. In this study, datasets were selected
based on their temporal coverage, spatial resolution, and relevance to the research objectives. Specifically, the 2017 Global
30-meter Wetland Dataset (GWL_FCS30) (Zhang et al., 2024) was utilized. Using AI Earth's integrated data processing tools,
the dataset was filtered to extract data corresponding to the required time periods, geographic regions, and variable subsets.
These preprocessing options ensured that only data pertinent to the study area were retained. The dataset was then clipped to
140   the predefined study region to reduce data volume and ensure spatial compatibility. Where necessary, advanced tools were
employed to perform coordinate system transformations. Overall, the nitrogen emission inventory and wetland type
distribution in East Asia adopted in this study are shown in **Fig. 1**.
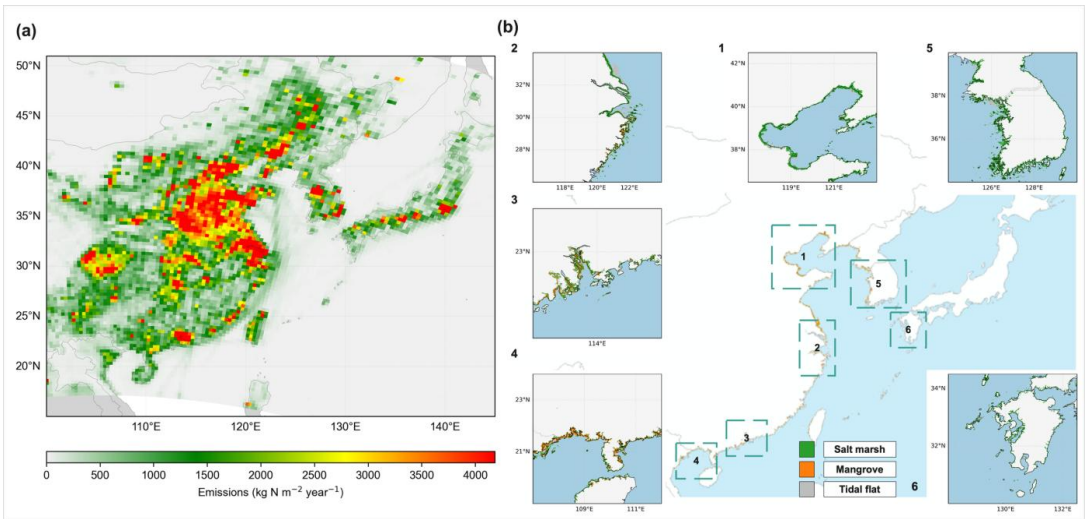
145   **Figure 1. Nitrogen emissions (a) and wetland type distribution (b) in East Asia. Different research areas in East Asia
have been marked with dotted lines.**

2.2 Atmospheric Deposition Model System Description

This study employed a mesoscale meteorological–chemical modelling framework to simulate the transport and deposition of
150   atmospheric nitrogen in coastal regions. Meteorological fields were generated using the Weather Research and Forecasting
(WRF) model version 4.1.1, driven by global atmospheric reanalysis data from the National Centers for Environmental
Prediction (NCEP) Final Operational Global Analysis (FNL), which serves as both the initial and boundary condition dataset.
The input data have a spatial resolution of 1° × 1° and a temporal resolution of 6 hours. The WRF physical parameterizations
included the Pleim–Xiu land surface model (Xiu and Pleim, 2001), the Rapid Radiative Transfer Model for General Circulation
155   Models (RRTMG) for both shortwave and longwave radiation schemes (Clough et al., 2005), the Asymmetric Convective
Model version 2 (ACM2) for planetary boundary layer (PBL) processes (Pleim, 2007), the Kain–Fritsch scheme for cumulus
parameterization (Kain, 2004), and MODIS-based land use classification data with 20 categories. The atmospheric chemistry
component was represented by the Community Multiscale Air Quality (CMAQ) model, developed by the U.S. Environmental
Protection Agency (EPA). CMAQ is a regional-to-hemispheric scale air quality model designed to simulate atmospheric
160   pollutant transport, chemical transformation, and deposition. In this study, CMAQ version 5.4 was used to estimate nitrogen
deposition in both oxidized and reduced forms. The model configuration incorporates the aero7 aerosol module (Xu et al.,
2018a) and the cb6r5 gas-phase chemical mechanism (Amedro et al., 2020), which includes detailed halogen chemistry. Dry
deposition processes were modelled using the M3Dry scheme (Pleim and Ran, 2011), which was updated in CMAQ v5.4 to

165 improve consistency with size-resolved particulate matter observations (Pleim et al., 2022). Wet deposition was calculated via the AQCHEM cloud chemistry module (Fahey et al., 2017). The simulation's initial and boundary conditions were based on seasonally averaged outputs from the hemispheric CMAQ dataset provided by the Community Modelling and Analysis System (CMAS) database (U.S. EPA: CMAQ Model Version 5.3 Input Data). The simulation domain covered the East Asian region, as illustrated in Fig. S1, with detailed parameter settings provided in Supplementary Section 1.2. The final landcover dataset was exported in GeoTIFF format for further processing in ArcGIS.

170

2.3 Calculation of Carbon Sequestration

Coastal wetlands in East Asia play a significant role in carbon sequestration. According to previous studies, 1 kg of carbon corresponds to approximately 2.2 kg of organic matter. Based on the chemical equations of photosynthesis, the production of 1 kg of organic matter leads to the fixation of approximately 1.63 kg of CO_2 and the release of 1.19 kg of O_2. Additionally, 1

175 kg of CO_2 contains about 0.27 kg of elemental carbon (Wang et al., 2005; Minghui et al., 2012). Using these stoichiometric relationships, annual carbon sequestration and oxygen release from wetland ecosystems can be estimated based on their net primary productivity (NPP).

The following equations were used to calculate carbon sequestration and oxygen release:

$$W_{CO2} = NPP \times 2.2 \times 1.63 \, , \tag{1}$$

180
$$W_C = W_{CO2} \times 0.27 \, , \tag{2}$$

$$W_O = NPP \times 2.2 \times 1.19 \, , \tag{3}$$

where W_{CO2} represents the amount of CO_2 fixed per unit area (g m^{-2}), Wc represents the carbon sequestration per unit area of wetland (g m^{-2}), NPP refers to the net primary productivity (g C m^{-2}) of vegetation per unit area per year, and Wo represents the oxygen release per unit area of wetland (g m^{-2}).

185 NPP was estimated using a modified Carnegie–Ames–Stanford Approach (CASA) model (Tang et al., 2024; Su et al., 2021), which simulates annual and seasonal NPP values based on remote sensing imagery and meteorological data. Seasonal values were extracted for January, April, July, and October to represent winter, spring, summer, and autumn, respectively. The CASA model, a light use efficiency model, integrates both environmental and biological factors—including effective solar radiation and vegetation-specific characteristics—to estimate NPP.

190 The basic structure of the CASA model is as follows:

$$NPP = APAR \times \varepsilon \, , \tag{4}$$

$$APAR = SOL \times FPAR \times 0.5 \, , \tag{5}$$

where absorb photosynthetically active radiation (APAR) represents the photosynthetically active radiation absorbed by the vegetation (MJ m^{-2}), ε is the light use efficiency (g C MJ^{-1}), SOLAR refers to the total monthly solar radiation (MJ/ m^2), FPAR

195 is the fraction of photosynthetically active radiation (FPAR) absorbed by the vegetation canopy, and the constant 0.5 represents the proportion of incoming solar radiation that is photosynthetically active. The light use efficiency ε was parameterized using values derived from existing literature. For forests, a value of 1.044 g C MJ^{-1} was used, while for salt marshes, a lower bound of 0.389 g C MJ^{-1} was adopted (Zhu et al., 2006). Monthly solar radiation data used in the model are listed in Supplementary Table S3.

200 ## 3 Results and Discussion

3.1 Nitrogen Deposition Flux in East Asian Coastal Wetlands

The nitrogen deposition flux in East Asian coastal wetlands exhibits significant source-specific heterogeneity. In terms of overall magnitude, terrestrial anthropogenic activities—such as industrial emissions, transportation, and agricultural

fertilization—contribute more substantially to atmospheric nitrogen input than marine vessel emissions. However, ship sources
205 still exert a notable influence on specific chemical forms and in particular spatial regions. The physical and chemical forms of
nitrogen play a crucial role in determining their atmospheric transport dynamics and deposition behaviour. Particulate nitrogen
species, such as NO_3^--N and NH_4^+-N, tend to exhibit higher deposition rates due to their relatively large particle sizes and
shorter atmospheric residence times. In contrast, gaseous nitrogen compounds like NO_x-N and NH_3-N can be transported over
longer distances and, following atmospheric chemical transformations, deposit over broader spatial scales through both dry
210 and wet pathways.

According to simulation results, nitrogen deposition fluxes from ship emissions were 60.86 mg N m^{-2} yr^{-1} for NO_3^--N, 17.27
for NH_4^+-N, 9.93 for NO_x-N, and 0.01 for NH_3-N, respectively (Table 1). These values correspond to contribution rates of
10.13 %, 15.22 %, 11.95 %, and 0.02 %. Although the contribution of ships to gaseous NH_3-N is negligible, they accounted
for over 10% of the total particulate nitrogen deposition (NO_3^--N and NH_4^+-N). This highlights the role of ship emissions in
215 the regional formation of nitrate aerosols and secondary particulate matter, especially in coastal atmospheric environments
where both dry and wet deposition processes are prevalent (Chen et al., 2024; Qiu et al., 2022). Deposition patterns also differ
significantly across various coastal wetland types. A comparative analysis of three representative wetlands—mangrove forests,
salt marshes, and tidal flats—reveals marked differences in gaseous nitrogen deposition. The deposition flux of NO_x-N in salt
marshes and tidal flat wetlands was found to be 24.71 % and 20.25 % higher, respectively, compared to that in mangrove
220 forests. In contrast, the deposition flux of NH_3-N was observed to be 17.13 % and 23.25 % lower in salt marshes and tidal flats,
respectively, when compared to mangrove forests. These discrepancies are likely attributed to variations in wetland distribution,
microclimatic conditions, and vegetation structure. Mangrove ecosystems, typically situated in estuarine regions, are
characterized by complex vegetation that enhances the capture of both particulate nitrogen and reactive gaseous nitrogen. Tidal
flats often function as atmospheric nitrogen "sinks" due to their proximity to riverine and marine interfaces (Wang et al., 2019).
225 In terms of total deposition flux, salt marsh wetlands exhibit the highest nitrogen input per unit area. The total deposition of
NO_3^--N and NH_4^+-N in salt marshes wetlands was 654.99 mg N m^{-2} yr^{-1} and 131.14 mg N m^{-2} yr^{-1}, respectively—approximately
17 % higher than in mangrove forests and 19% higher than in tidal flats. However, because the areal extent of mangrove
wetlands is limited, their contribution to regional nitrogen input is lower than that of more widespread salt marsh and tidal flat
systems. This suggests that regional nitrogen budgets may not rely solely on per-area deposition rates; spatial distribution and
230 wetland coverage should also be incorporated to accurately assess ecological carrying capacity and nitrogen input pressure.

In summary, nitrogen deposition in East Asian coastal wetlands is governed by an interplay of emission source type and
nitrogen chemical form. While land-based pollutants are the dominant drivers of regional nitrogen deposition, shipborne
emissions—particularly those contributing to particulate nitrogen—play a non-negligible role in coastal boundary zones.

235 **Table 1. The totally different source of nitrogen deposition in different wetlands (Unit: mg N m^{-2} year^{-1})**

	Sources	Salt marsh	Mangrove forest	Tidal flat	All
	Anthropogenic	588.97	516.69	534.99	540.11
NO_3^--N	Marine ship	66.02	43.07	60.99	60.86
	Total	654.99	559.76	595.98	600.97
	Anthropogenic	112.20	118.86	93.17	96.23
NH_4^+-N	Marine ship	18.94	16.16	17.11	17.27
	Total	131.14	135.02	110.28	113.50
	Anthropogenic	77.01	62.21	73.19	73.20
NO_x-N	Marine ship	9.40	7.08	10.13	9.93
	Total	86.41	69.29	83.32	83.13
	Anthropogenic	59.96	72.36	55.54	56.67

|					
NH$_3$-N	Marine ship	0.01	0.01	0.01	0.01
	Total	59.98	72.38	55.55	56.68

Note: The last column of the table represents the nitrogen deposition flux for each wetland type, which is the weighted average value calculated based on the area proportion of each wetland.

3.2 Spatial Temporal Differences in Nitrogen Deposition Fluxes of Different Coastal Wetlands in East Asia

3.2.1 Spatial Characteristics of Nitrogen Deposition in East Asian Coastal Wetlands

240   Spatial distribution maps of nitrogen deposition across six coastal wetland regions in East Asia revealed a general gradient characterized by "higher in the west, lower in the east" and "stronger in the south, weaker in the north" (**Fig. 2**). The distribution of nitrogen deposition points across countries is further illustrated in Supplementary Fig. S1. Among the six regions, the YRD, Pearl River Delta (PRD), and Beibu Gulf (BG) exhibited the highest nitrogen deposition fluxes, with localized values exceeding 10 g N·m^{-2} yr^{-1}, highlighting substantial anthropogenic influence in these areas. In the Bohai Bay (BS), although

245   the overall nitrogen deposition intensity is slightly lower than that in southern regions, industrial clusters near cities such as Tianjin and Tangshan show distinctly elevated fluxes. Wetlands on the western KP and Japan's Kyushu Island had scattered patterns of low to moderate nitrogen deposition that were largely influenced by atmospheric transport and local topography.
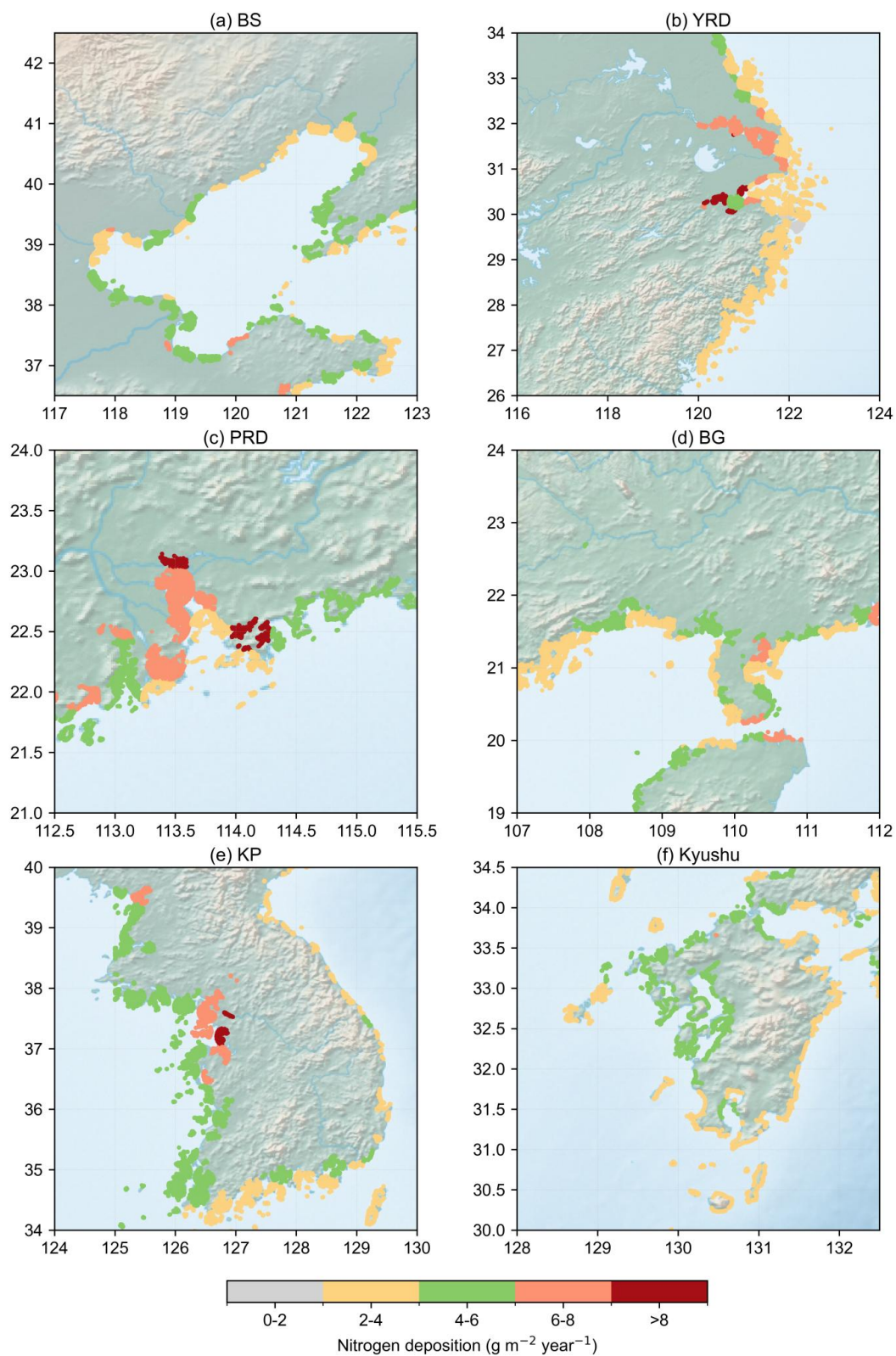
250 **Figure 2. Spatial Distribution of annual total atmospheric nitrogen deposition in coastal wetlands across different regions of East Asia (g N m^{-2} yr^{-1}). BS means Bohai Bay, YRD means the Yangtze River Delta, PRD means Pearl River Delta, BG means Beibu Gulf, KP means the Korean Peninsula, and Kyushu means the Kyushu of Japan.**

255 Moderate nitrogen deposition is typical for the wetlands of BS, but some areas, especially near the Beijing-Tianjin-Hebei urban agglomeration, could exceed 8 g N m^{-2} yr^{-1}. Fluctuations in wetlands on the Shandong Peninsula, especially in the Bohai Bay area, are significantly higher than those in other parts of the bay. In the YRD, nitrogen deposition rates typically ranged from 2 to 4 g N m^{-2} yr^{-1}, with the highest values predominantly observed in riverine and coastal zones such as the Yangtze River estuary, Hangzhou Bay, and the Zhejiang coastal region. These elevated deposition levels were likely attributable to the dense distribution of emission sources in industrialized and urbanized areas. Similarly, wetlands in the PRD exhibited considerable

260 nitrogen deposition, particularly in the Pearl River Estuary, where concentrations increased with proximity to an inland urban centre. This spatial pattern reflects the combined influence of industrial activities and maritime shipping. The ten key strategic pillar industries of Guangdong Province were largely concentrated in this core region, and major ports such as Guangzhou, Shenzhen, and Zhuhai constitute a globally significant maritime hub. Consequently, ship emissions contributed significantly to the observed nitrogen deposition. The wetlands demonstrated a distinct spatial pattern characterized as "combined land-sea

265 source influence with regional retention effects." In cities including Nanning, Fangchenggang, Qinzhou, and Beihai, average nitrogen deposition was approximately 0.69 g N m^{-2} yr^{-1}, with peak values ranging between 6 and 8 g N m^{-2} yr^{-1}. In contrast, coastal wetlands on the KP generally experience lower nitrogen input levels, although higher deposition rates are observed on certain offshore islands, likely due to localized accumulation and long-range atmospheric transport. On a regional scale, nitrogen deposition in the KP showed a tendency to accumulate in northern and inland areas, potentially influenced by

270 transboundary transport from China and local emission sources. On Kyushu Island in Japan, nitrogen deposition was primarily in the form of NO$_3^-$-N, with an average flux of approximately 0.14 g N m^{-2} yr^{-1}. Elevated deposition levels were mainly found along the northwestern coastline and in the northern regions of the island, likely driven by atmospheric transport from coastal Chinese regions and anthropogenic activities on adjacent Japanese islands.

In summary, nitrogen deposition across East Asian coastal wetlands exhibited marked spatial heterogeneity driven by a

275 combination of land-based emissions, maritime shipping lanes, atmospheric transport, and geographic/topographic factors. Coastal regions such as the YRD and PRD, which are economically dynamic, experience the highest levels of nitrogen input. Meanwhile, the BS and BG display more uneven and spatially fragmented deposition patterns. Wetlands in the KP and Kyushu Island, while exhibiting lower overall fluxes, reflected the influence of long-range nitrogen transport and localized accumulation. These findings emphasize the need for region-specific nitrogen management strategies that account for both

280 emission source profiles and spatial variability in ecosystem sensitivity.

3.2.2 Dry and Wet Deposition Fluxes and Seasonal Characteristics of Nitrogen in Coastal Wetlands of East Asia

Nitrogen deposition in coastal wetlands primarily occurs through two mechanisms: wet and dry deposition. Wet deposition involves the removal of atmospheric nitrogen compounds—both gaseous and particulate—via precipitation (such as rain or

285 snow), occurring mainly through in-cloud (rainout) and below-cloud scavenging processes. In contrast, dry deposition refers to the direct transfer of nitrogen species (e.g., gaseous or particulate NO$_x$ and NH$_3$) to the Earth's surface in the absence of precipitation, facilitated by gravitational settling, turbulent diffusion, or gas absorption. As previously outlined, nitrate (NO$_3^-$_N) and ammonium (NH$_4^+$_N) constituted the dominant forms of nitrogen deposition in East Asian coastal wetlands, while the direct dry deposition of gaseous NOx and NH$_3$ contributed only 6.63 % and 9.73 % of total deposition, respectively.

290 Building upon this, the present study further investigated the seasonal variation in nitrate and ammonium deposition, distinguishing between wet and dry fluxes across six representative regions (**Fig. 3**). Overall, nitrate deposition consistently surpasses ammonium deposition in all regions, reinforcing its dominant role in nitrogen input. Moreover, wet deposition was identified as the primary contributor across all areas, significantly exceeding dry deposition—underscoring the critical influence of seasonal rainfall on nitrogen dynamics in these ecosystems.
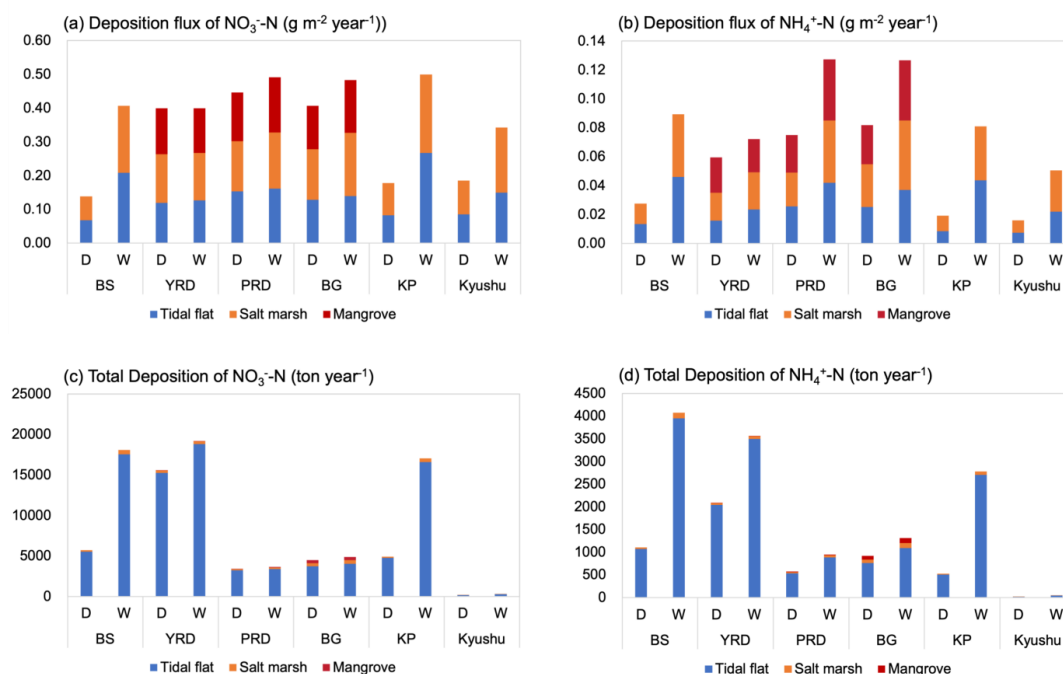
Figure 3. Average dry and wet deposition fluxes of nitrate and ammonium nitrogen (a, b), and the total annual nitrogen deposition (c, d) in six typical wetland regions.

However, the degree of difference between dry and wet deposition varies significantly among regions. For instance, the KP exhibited the most pronounced seasonal asymmetry in nitrate deposition, with wet deposition exceeding dry deposition by 0.17 g N·m^{-2} yr^{-1}. A similarly marked difference was observed in the BS, where the nitrate wet-dry gap reaches 0.14 g N·m^{-2} yr^{-1}, reflecting the combined influence of seasonal precipitation and emission intensity. The YRD distinguished itself with a relatively balanced level of ammonium nitrogen deposition, exhibiting a minimal dry-wet deposition difference of merely 0.05 g N m^{-2} yr^{-1}, which was the smallest among all six evaluated regions. This phenomenon can be attributed to the region's stable atmospheric humidity, consistent sources of ammonia—such as agricultural activities and wastewater—and high vegetation cover, which facilitates enhanced nitrogen absorption under both dry and wet conditions.

In other words, even within regions that share similar latitudinal positions and ecological characteristics, the ratio of dry to wet deposition can exhibit significant variation due to differences in atmospheric circulation patterns, precipitation regimes, and land-sea interactions. For example, Kyushu Island in Japan demonstrated the lowest overall nitrogen deposition among the six study areas examined. The annual fluxes of dry and wet deposition for nitrate nitrogen and ammonium nitrogen amounted to only 183.92 tons, 337.05 tons, 15.45 tons, and 49.24 tons, respectively. This relatively low input of nitrogen is likely a consequence of limited industrial emissions coupled with the predominant influence of clean maritime air masses originating from upwind oceanic regions. (Hayashi et al., 2021; Kiriyama et al., 2021).

Focusing on specific types of wetlands, mangrove ecosystems consistently showed higher fluxes of both nitrate and ammonium nitrogen compared to salt marshes and tidal flats across most regions. This phenomenon may be attributed to their dense canopy structure, increased surface roughness, and complex vertical stratification, all of which significantly enhance nitrogen retention capacity. (Qian et al., 2023; Alongi, 2020). Furthermore, the proximity of numerous mangrove wetlands to urban and industrial sources likely contributes to elevated localized nitrogen loads. In contrast, tidal flats—often characterized by sparse vegetation—exhibit higher absolute fluxes of dry and wet deposition in some regions. This may be attributed to their increased surface exposure and closeness to estuarine mixing zones, where atmospheric deposition readily interacts with open surfaces.
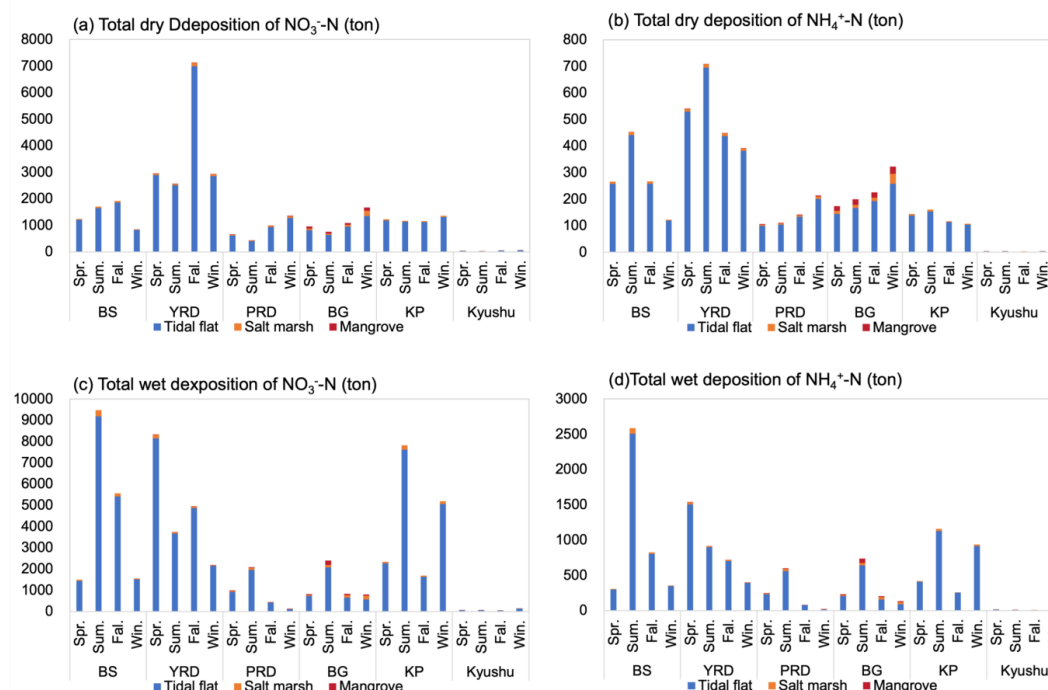
Figure 4. Seasonal Characteristics of Total Nitrogen Deposition in Six Typical Regions. (a) and (c) show the total dry and wet deposition of nitrate nitrogen in different typical regions across different seasons; (b) and (d) show the total dry and wet deposition of ammonium nitrogen in different typical regions across different seasons.

325

Seasonal patterns of total nitrogen deposition also vary substantially across coastal regions (**Fig. 4**). For instance, in the YRD, the dry deposition of nitrate nitrogen reached its peak during autumn, amounting to approximately 7139.55 tons. This increase is closely linked to heightened regional NO_x emissions resulting from fossil fuel combustion, along with specific meteorological conditions such as a shallower planetary boundary layer that facilitates the accumulation and surface deposition

330 of atmospheric nitrogen. In contrast, ammonium nitrogen dry deposition in the same region does not demonstrate a similar autumnal peak. This discrepancy is likely attributable to its stronger association with agricultural sources and their seasonally variable application cycles. (Liu et al., 2011).

In the BG, a distinct seasonal profile was observed. Here, dry deposition of both nitrate and ammonium nitrogen peaked in winter, which were 1667.85 tons and 322.32 tons respectively. This seasonal enhancement was likely driven by a combination

335 of long-range pollutant transport via the East Asian winter monsoon, frequent atmospheric inversion events, and limited vertical mixing along the coast, all of which amplify nitrogen loading during the winter season (Lao et al., 2021).

Regarding wet deposition, a more consistent pattern was observed in the BS, YRD, PRD, and BG wetlands. In these regions, spring and summer seasons exhibited significantly higher deposition fluxes compared to autumn and winter. This seasonal increase aligns with enhanced convective activity and frequent rainfall events that facilitate the scavenging of soluble nitrogen

340 compounds from the atmosphere. In contrast, Kyushu Island and the KP demonstrated relatively minor seasonal variations in wet deposition fluxes for both nitrate and ammonium nitrogen, indicating a more uniform annual distribution. This smooth intra-annual profile was likely attributable to the maritime climate characteristic of these island regions, which features moderate temperature gradients and evenly distributed precipitation throughout the year. (Zhao et al., 2015; Morino et al., 2011). Above all, nitrogen deposition in East Asian coastal wetlands demonstrated significant variation across regions, seasons,

345 and wetland types. Wet deposition of particulate nitrogen consistently surpassed dry deposition, with seasonal variations—especially during the spring and summer—playing a pivotal role in shaping both the magnitude and pathways of nitrogen input.

3.3 Potential Impacts of Atmospheric Nitrogen Deposition on Carbon Sequestration Capacity

Utilizing remote sensing data and ecological model outputs from six representative coastal regions in East Asia, this study systematically evaluates the seasonal dynamics of NPP and CO_2 fixation across three wetland types—mangrove forests, salt

350 marshes, and tidal flats—during spring, summer, autumn, and winter (**Fig. 5**). Among these wetland types, mangrove forests exhibited superior performance across all metrics, highlighting their crucial role as "blue carbon" ecosystems with significant carbon sequestration potential. During summer, mangrove forests received an average solar radiation of 1650.80 MJ m^{-2} and APAR of 701.59 MJ m^{-2}, resulting in a high mean NPP of 732.47 g C m^{-2}. Corresponding CO_2 fixation and O_2 release reached 2626.62 g m^{-2-2} and 3061.71 g m^{-2}, respectively (Fig. 5a and Table S4). FPAR for mangrove forests remained stable around

355 0.85 throughout the year, substantially higher than salt marshes (~0.65) and tidal flats (<0.15), indicating a pronounced advantage in light use efficiency. This advantage arises from mangrove forests' evergreen habit, complex canopy structure, and higher water availability, which sustain efficient photosynthesis under high temperature and humidity conditions (Barr et al., 2013).
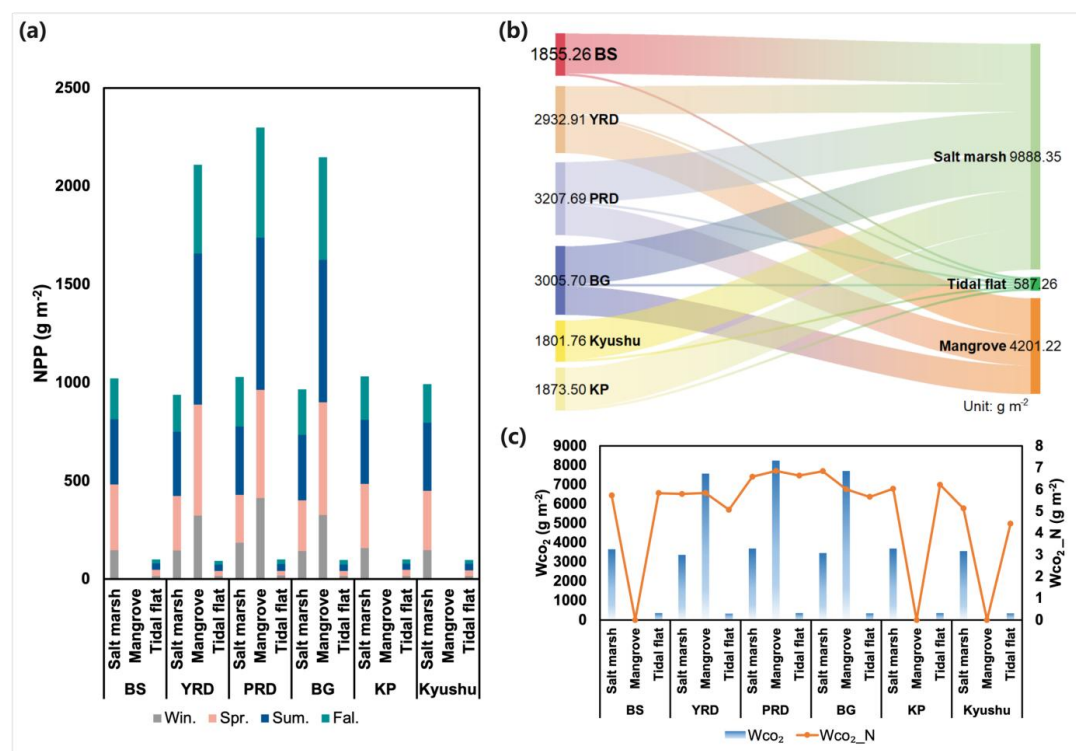

360

Figure 5. NPP and carbon sequestration in different wetland types across various regions. (a) is the total NPP across four seasons for different wetland types in each region; the Sankey diagram shows the NPP distribution of the three types of wetlands in various regions (b); (c) is the annual total carbon sequestration and nitrogen deposition-induced carbon sequestration in different wetland types across regions.

365

In contrast, mangrove—common in temperate and subtropical coastal zones—exhibit intermediate carbon sequestration capacity (Fig. 5b). For instance, mangrove forests in the YRD had a summer APAR of approximately 563.3 MJ m^{-2}, corresponding to an NPP of 342.5 g C m^{-2}, CO_2 fixation of 1228.2 g m^{-2}, and O_2 release of 1431.6 g m^{-2}. These values, though lower than those of the salt marsh, surpass those of tidal flats. Salt marsh vegetation—including species such as Phragmites

370 australis and Suaeda salsa—comprises seasonal herbaceous plants with short life cycles. The photosynthetic activity and carbon accumulation of these plants are significantly influenced by seasonal variations in hydrology, salinity, and

anthropogenic disturbances (Qiu et al., 2019a; Li et al., 2016).

Tidal flats, characterized by sparse or exposed vegetation cover, demonstrated the weakest carbon sequestration metrics. In winter, for example, APAR in tidal flats of the BS can decrease to 37.2 MJ m^{-2}, with NPP falling to 14.5 g C m^{-2}, and CO_2

375   fixation and O_2 release declining to 51.9 g m^{-2} and 37.9 g m^{-2}, respectively. These low values align with the consistently low FPAR (<0.1), reflecting the limited photosynthetic contribution of tidal flats.

At the regional scale, a distinct north-to-south gradient in carbon sequestration capacity is evident (Fig. 5c). The YRD and the PRD, located within tropical and southern subtropical climates, benefit from higher annual solar radiation and more stable light conditions. These factors contribute to extended growing seasons and enhanced productivity of wetlands. For instance,

380   mangrove forests in the region maintained the NPP exceeding 500 g C m^{-2} during spring, summer, and autumn. In contrast, the NPP values of mangrove forests located in the YRD and BG regions were slightly lower. The limited winter solar radiation in these areas (total radiation < 745.00 MJ m^{-2}), combined with a relatively high temperature threshold for salt marsh growth, significantly restricts photosynthetic activity. Conversely, mangrove forests sustained a winter NPP of 326.13 g C m^{-2}, demonstrating notable cold tolerance and stability as carbon sinks. Similarly, salt marshes and tidal flats within both the YRD

385   and PRD exhibited elevated APAR and NPP values. This reinforces the conclusion that temperature and solar radiation serve as key external drivers limiting carbon sequestration in coastal wetlands.

Seasonally, carbon sequestration exhibited peaks during the summer across all wetland types, primarily driven by maximal solar elevation angles, extended daylight hours, and increased radiation intensity. For example, the highest NPP of mangrove forests in summer reached 776.16 g C m^{-2}, approximately double that of winter values. This pronounced seasonal variation is

390   even more pronounced in salt marshes and tidal flats, where NPP approaches near-zero levels during autumn and winter. Notably, in regions such as the PRD, mangrove NPP in autumn slightly exceeds spring values, likely attributable to nutrient inputs from post-typhoon events and heavy rainfall that temporarily enhance photosynthetic efficiency and biomass accumulation. (Qiu et al., 2019b). Regional disparities in seasonal responses further underscore wetland ecosystems' sensitivity to localized climate and hydrological factors.

395   The influence of nitrogen deposition on carbon sequestration also shows marked seasonal and regional variability. The regulatory effect of nitrogen input on carbon sequestration is more pronounced during the warm season (April to October), when wetland vegetation exhibits heightened photosynthetic potential and nutrient uptake efficiency. For example, in PRD mangrove forests, nitrogen deposition increases carbon sequestration by up to 6.85 g m^{-2} during summer, accounting for approximately 0.1 % of total seasonal carbon sequestration; however, this effect diminishes to below 0.06 % in winter. This

400   seasonal disparity likely results from low winter temperatures limiting nitrogen mineralization and plant assimilation, thereby constraining nitrogen's regulatory role. Salt marshes display similar seasonal trends but with comparatively lower nitrogen responsiveness, indicating lower sensitivity to exogenous nutrient inputs than mangrove forests. Additionally, in regions with high background nitrogen levels—such as the Yangtze River Delta and Taiwan's western coast—the marginal enhancement of carbon sequestration by nitrogen deposition tends to plateau, suggesting the onset of nitrogen saturation effects (Lu et al.,

405   2021).

4. Conclusions

This study utilized the WRF-CMAQ model, integrating multi-source emission inventories and high-resolution wetland land cover data, to comprehensively assess nitrogen deposition flux characteristics and their ecological impacts in East Asian coastal wetlands. The main findings are as follows:

410   Terrestrial anthropogenic emissions—primarily from industry, transportation, and agriculture—remain the predominant contributors to nitrogen deposition. Deposition fluxes of particulate and gaseous nitrogen species from these sources far exceed those from ship emissions. Nonetheless, ship emissions contribute notably to particulate nitrogen deposition, accounting for 10.13 % of NO_3^--N and 15.22 % of NH_4^+-N fluxes, underscoring their regional significance in nitrate and ammonium aerosol formation, especially in coastal zones with intensive port activities and complex wet/dry deposition dynamics.

415   On a per-unit-area basis, salt marshes of the East Asia region coastal wetland exhibit the highest nitrogen deposition fluxes, significantly surpassing mangrove forests and tidal flats. However, due to their relatively limited spatial extent, mangrove

forests receive less of the total regional nitrogen inputs compared to the more extensive salt marshes and tidal flats. This highlights the importance of considering both per-area flux and overall coverage when evaluating nitrogen deposition pressure. Wetland-specific deposition patterns reveal that NO_x-N deposition is roughly 20 % higher in mangrove forests and tidal flats

420 than in salt marshes, whereas NH_3-N deposition is more pronounced in salt marshes. The PRD, YRD, and BG emerge as nitrogen deposition hotspots, with annual fluxes exceeding 10 g N m^{-2}—markedly higher than levels observed in the KP and Kyushu coastal regions. The PRD, in particular, exhibits the highest nitrogen load due to a combination of dense industrial emissions and a globally significant port cluster, resulting in elevated atmospheric nitrogen driven by both terrestrial and maritime sources, establishing a characteristic nitrogen deposition core in port-industrial complexes.

425 Marked seasonal and spatial disparities characterize nitrogen deposition dynamics. In the YRD, dry nitrate deposition peaks in autumn at approximately 7139.55 tons, driven by fossil fuel emissions and atmospheric stagnation, whereas wet deposition in the BS and BG can exceed 60 % of annual input during spring and summer. Wetland type also matters: mangrove wetlands receive up to twice the nitrogen fluxes of nearby salt marshes, due to higher canopy roughness and urban proximity.

Carbon sequestration exhibits clear spatial and temporal heterogeneity in response to atmospheric depositions, with southern

430 wetlands displaying greater sink potential than northern counterparts. Mangrove forests in tropical regions sustain high NPP year-round (above 500 g C m^{-2} in spring, summer, and autumn). Seasonal carbon sequestration peaks in summer, driven by increased solar radiation and day length. Nitrogen deposition further enhances carbon uptake during the warm season—for example, increasing carbon sequestration by 6.85 g m^{-2} in PRD mangrove forests—though this effect weakens in winter. In regions with high nitrogen load, signs of nitrogen saturation are evident, signalling the need for future nitrogen management

435 strategies that account for both regional variability and spatiotemporal dynamics of nitrogen inputs.

This study establishes a connection between atmospheric nitrogen input into coastal wetlands and the natural carbon reservoir, thereby enhancing our understanding of nutrient sources and mechanisms within coastal ecosystems that play a crucial role in mitigating climate change. Furthermore, these findings provide an alternative perspective on the potential impacts of nitrogen management stemming from anthropogenic activities.

440 **Code/Data availability**

Author contribution

JL and YX analyzed the data; JL wrote the manuscript draft; SJ provided emission inventory data; YZ, YX, CJ, QY and WM reviewed and edited the manuscript.

Competing interests

450 The authors declare that they have no conflict of interest.

Acknowledgement

455 **Reference**

Adam Langley, J., Mozdzer, T. J., Shepard, K. A., Hagerty, S. B., and Patrick Megonigal, J.: Tidal marsh plant responses to elevated CO2, nitrogen fertilization, and sea level rise, Glob. Change Biol., 19, 1495–1503, https://doi.org/10.1111/gcb.12147, 2013.

Alongi, D. M.: Carbon Balance in Salt Marsh and Mangrove Ecosystems: A Global Synthesis, J. Mar. Sci. Eng., 8, 767,
460 https://doi.org/10.3390/jmse8100767, 2020.

Amedro, D., Berasategui, M., Bunkan, A. J. C., Pozzer, A., Lelieveld, J., and Crowley, J. N.: Kinetics of the OH + NO$_2$ reaction: effect of water vapour and new parameterization for global modelling, Atmospheric Chem. Phys., 20, 3091–3105, https://doi.org/10.5194/acp-20-3091-2020, 2020.

Bange, H. W.: Nitrous oxide and methane in European coastal waters, Estuar. Coast. Shelf Sci., 70, 361–374,
465 https://doi.org/10.1016/j.ecss.2006.05.042, 2006.

Barbier, E. B., Hacker, S. D., Kennedy, C., Koch, E. W., Stier, A. C., and Silliman, B. R.: The value of estuarine and coastal ecosystem services, Ecol. Monogr., 81, 169–193, https://doi.org/10.1890/10-1510.1, 2011.

Barnes, J. and Upstill-Goddard, R. C.: N2O seasonal distributions and air-sea exchange in UK estuaries: Implications for the tropospheric N2O source from European coastal waters, J. Geophys. Res. Biogeosciences, 116,
470 https://doi.org/10.1029/2009JG001156, 2011.

Barr, J. G., Engel, V., Fuentes, J. D., Fuller, D. O., and Kwon, H.: Modeling light use efficiency in a subtropical mangrove forest equipped with CO$_2$ eddy covariance, Biogeosciences, 10, 2145–2158, https://doi.org/10.5194/bg-10-2145-2013, 2013.

Chakraborty, S. K.: Bioinvasion and Environmental Perturbation: Synergistic Impact on Coastal–Mangrove Ecosystems of West Bengal, India, in: Impacts of Invasive Species on Coastal Environments: Coasts in Crisis, edited by: Makowski, C. and
475 Finkl, C. W., Springer International Publishing, Cham, 171–245, https://doi.org/10.1007/978-3-319-91382-7_6, 2019.

Chen, B. and Sun, Z.: Effects of nitrogen enrichment on variations of sulfur in plant-soil system of *Suaeda salsa* in coastal marsh of the Yellow River estuary, China, Ecol. Indic., 109, 105797, https://doi.org/10.1016/j.ecolind.2019.105797, 2020.

Chen, J., Fu, X., Wang, X., Dong, S., Chen, T., Xue, L., Zhou, Y., Sheng, L., and Wang, W.: Unveiling the overlooked direct emissions of particulate organic nitrates from ship, Environ. Int., 185, 108487, https://doi.org/10.1016/j.envint.2024.108487,
480 2024.

Cheng, S., Fang, H., Xu, M., Geng, J., He, S., Yu, G., and Cao, Z.: Regulation of plant-soil-microbe interactions to soil organic carbon in natural ecosystems under elevated nitrogen deposition: A review, Acta Ecol. Sin., 38, 8285–8295, https://doi.org/10.5846/stxb201709011581, 2018.

Clough, S. A., Shephard, M. W., Mlawer, E. J., Delamere, J. S., Iacono, M. J., Cady-Pereira, K., Boukabara, S., and Brown, P.
485 D.: Atmospheric radiative transfer modeling: a summary of the AER codes, J. Quant. Spectrosc. Radiat. Transf., 91, 233–244, https://doi.org/10.1016/j.jqsrt.2004.05.058, 2005.

Deegan, L. A., Johnson, D. S., Warren, R. S., Peterson, B. J., Fleeger, J. W., Fagherazzi, S., and Wollheim, W. M.: Coastal eutrophication as a driver of salt marsh loss, Nature, 490, 388–392, https://doi.org/10.1038/nature11533, 2012.

Fahey, K. M., Carlton, A. G., Pye, H. O. T., Baek, J., Hutzell, W. T., Stanier, C. O., Baker, K. R., Appel, K. W., Jaoui, M., and
490 Offenberg, J. H.: A framework for expanding aqueous chemistry in the Community Multiscale Air Quality (CMAQ) model version 5.1, Geosci. Model Dev., 10, 1587–1605, https://doi.org/10.5194/gmd-10-1587-2017, 2017.

Fan, Q., Zhang, Y., Ma, W., Ma, H., Feng, J., Yu, Q., Yang, X., Ng, S. K. W., Fu, Q., and Chen, L.: Spatial and Seasonal Dynamics of Ship Emissions over the Yangtze River Delta and East China Sea and Their Potential Environmental Influence, Environ. Sci. Technol., 50, 1322–1329, https://doi.org/10.1021/acs.est.5b03965, 2016.

495 Fettrow, S., Wozniak, A., Michael, H. A., and Seyfferth, A. L.: Factors controlling spatiotemporal variability of soil carbon accumulation and stock estimates in a tidal salt marsh, Biogeosciences, 21, 2367–2384, https://doi.org/10.5194/bg-21-2367-2024, 2024.

Fu, G., Qi, Y., Li, J., Zhao, C., He, J., Ma, Y., and Zhu, J.: Spatial Distributions of Nitrogen and Phosphorus in Surface Sediments in Intertidal Flats of the Yellow River Delta, China, Water, 13, 2899, https://doi.org/10.3390/w13202899, 2021.

500 Goldberg, L., Lagomasino, D., Thomas, N., and Fatoyinbo, T.: Global declines in human-driven mangrove loss, Glob. Change Biol., 26, 5844–5855, https://doi.org/10.1111/gcb.15275, 2020.

Gruber, N. and Galloway, J. N.: An Earth-system perspective of the global nitrogen cycle, Nature, 451, 293–296, https://doi.org/10.1038/nature06592, 2008.

Hayashi, K., Shibata, H., Oita, A., Nishina, K., Ito, A., Katagiri, K., Shindo, J., and Winiwarter, W.: Nitrogen budgets in Japan

505 from 2000 to 2015: Decreasing trend of nitrogen loss to the environment and the challenge to further reduce nitrogen waste, Environ. Pollut., 286, 117559, https://doi.org/10.1016/j.envpol.2021.117559, 2021.

Hong, S., Liu, Z., Zhang, G., Cai, Y., Wang, Q., Zhang, C., and Song, C.: Distribution of habitat suitability for *Suaeda salsa* in the Liaohe River Estuary and its relationship with carbon storage, Sci. Total Environ., 954, 176092, https://doi.org/10.1016/j.scitotenv.2024.176092, 2024.

510 Hu, M., Peñuelas, J., Sardans, J., Huang, J., Li, D., and Tong, C.: Effects of nitrogen loading on emission of carbon gases from estuarine tidal marshes with varying salinity, Sci. Total Environ., 667, 648–657, https://doi.org/10.1016/j.scitotenv.2019.02.429, 2019.

Huang, X., He, Z., Wang, Y., Wang, F., Zheng, Z., Zuo, Y., Cao, Y., Yao, X., She, Z., Ge, Y., and Li, Y.: Assessment of soil microbial communities and diversity in typical coastal wetlands along a succession gradient: Implications for reconstructing

515 the long-term evolution of coastal wetlands, Environ. Technol. Innov., 39, 104263, https://doi.org/10.1016/j.eti.2025.104263, 2025.

Kain, J. S.: The Kain–Fritsch Convective Parameterization: An Update, 2004.

Kiriyama, H., Matsuda, H., Kamiji, Y., and Morita, S.: Nitrogen stock and farmer behaviour under rice policy change in Japan, J. Environ. Manage., 299, 113438, https://doi.org/10.1016/j.jenvman.2021.113438, 2021.

520 Lao, Q., Liu, G., Gao, J., Shen, Y., Su, Q., Chen, C., and Chen, F.: Seasonal Sources and Cycling of Nitrogen Revealed by Stable Isotopes in the Northeastern Beibu Gulf, China, J. Mar. Sci. Eng., 9, 1123, https://doi.org/10.3390/jmse9101123, 2021.

Leidner, A. K. and Buchanan, G. M. (Eds.): Satellite Remote Sensing for Conservation Action: Case Studies from Aquatic and Terrestrial Ecosystems, 1st ed., Cambridge University Press, https://doi.org/10.1017/9781108631129, 2018.

Li, L., Qiu, S., Chen, Y., Xu, X., Zhao, X., Christie, P., and Xu, M.: Allocation of photosynthestically-fixed carbon in plant and

525 soil during growth of reed (Phragmites australis) in two saline soils, Plant Soil, 404, 277–291, https://doi.org/10.1007/s11104-016-2840-2, 2016.

Li, M., Liu, H., Geng, G., Hong, C., Liu, F., Song, Y., Tong, D., Zheng, B., Cui, H., Man, H., Zhang, Q., and He, K.: Anthropogenic emission inventories in China: a review, Natl. Sci. Rev., 4, 834–866, https://doi.org/10.1093/nsr/nwx150, 2017a.

Li, M., Zhang, Q., Kurokawa, J., Woo, J.-H., He, K., Lu, Z., Ohara, T., Song, Y., Streets, D. G., Carmichael, G. R., Cheng, Y.,

530 Hong, C., Huo, H., Jiang, X., Kang, S., Liu, F., Su, H., and Zheng, B.: MIX: a mosaic Asian anthropogenic emission inventory under the international collaboration framework of the MICS-Asia and HTAP, Atmospheric Chem. Phys., 17, 935–963, https://doi.org/10.5194/acp-17-935-2017, 2017b.

Li, X., Bellerby, R., Craft, C., and Widney, S. E.: Coastal wetland loss, consequences, and challenges for restoration, Anthr. Coasts, 1, 1–15, https://doi.org/10.1139/anc-2017-0001, 2018.

535 Li, X., Zhang, X., Qiu, C., Duan, Y., Liu, S., Chen, D., Zhang, L., and Zhu, C.: Rapid Loss of Tidal Flats in the Yangtze River Delta since 1974, Int. J. Environ. Res. Public. Health, 17, 1636, https://doi.org/10.3390/ijerph17051636, 2020.

Liu, X., Duan, L., Mo, J., Du, E., Shen, J., Lu, X., Zhang, Y., Zhou, X., He, C., and Zhang, F.: Nitrogen deposition and its ecological impact in China: An overview, Environ. Pollut., 159, 2251–2264, https://doi.org/10.1016/j.envpol.2010.08.002, 2011.

540 Liu, X., Zhang, Y., Han, W., Tang, A., Shen, J., Cui, Z., Vitousek, P., Erisman, J. W., Goulding, K., Christie, P., Fangmeier, A., and Zhang, F.: Enhanced nitrogen deposition over China, Nature, 494, 459–462, https://doi.org/10.1038/nature11917, 2013.

Lu, X., Vitousek, P. M., Mao, Q., Gilliam, F. S., Luo, Y., Turner, B. L., Zhou, G., and Mo, J.: Nitrogen deposition accelerates soil carbon sequestration in tropical forests, Proc. Natl. Acad. Sci., 118, e2020790118, https://doi.org/10.1073/pnas.2020790118, 2021.

545 Marchant, H. K., Tegetmeyer, H. E., Ahmerkamp, S., Holtappels, M., Lavik, G., Graf, J., Schreiber, F., Mussmann, M., Strous, M., and Kuypers, M. M. M.: Metabolic specialization of denitrifiers in permeable sediments controls N2O emissions, Environ. Microbiol., 20, 4486–4502, https://doi.org/10.1111/1462-2920.14385, 2018.

Minghui, C., Yingbiao, C., Guanhua, G., and Bin, A.: Ecological Property Assessment in the Rapidly Urbanized Region Based

on RS: A Case Study of Dongguan, Ziranziyuan Xuebao, 27, 601–613, 2012.

550 Morino, Y., Ohara, T., Kurokawa, J., Kuribayashi, M., Uno, I., and Hara, H.: Temporal variations of nitrogen wet deposition across Japan from 1989 to 2008, J. Geophys. Res. Atmosheres, 116, https://doi.org/10.1029/2010JD015205, 2011.

Morris, J. T.: Effects of Nitrogen Loading on Wetland Ecosystems with Particular Reference to Atmospheric Deposition, Annu. Rev. Ecol. Syst., 22, 257–279, 1991.

Morris, J. T. and Bradley, P. M.: Effects of nutrient loading on the carbon balance of coastal wetland sediments, Limnol.
555 Oceanogr., 44, 699–702, https://doi.org/10.4319/lo.1999.44.3.0699, 1999.

Pleim, J. and Ran, L.: Surface Flux Modeling for Air Quality Applications, Atmosphere, 2, 271–302, https://doi.org/10.3390/atmos2030271, 2011.

Pleim, J. E.: A Combined Local and Nonlocal Closure Model for the Atmospheric Boundary Layer. Part I: Model Description and Testing, J. Appl. Meteorol. Climatol., 46, 1383, https://doi.org/10.1175/JAM2539.1, 2007.

560 Pleim, J. E., Ran, L., Saylor, R. D., Willison, J., and Binkowski, F. S.: A New Aerosol Dry Deposition Model for Air Quality and Climate Modeling, J. Adv. Model. Earth Syst., 14, e2022MS003050, https://doi.org/10.1029/2022MS003050, 2022.

Porter, E. M., Bowman, W. D., Clark, C. M., Compton, J. E., Pardo, L. H., and Soong, J. L.: Interactive effects of anthropogenic nitrogen enrichment and climate change on terrestrial and aquatic biodiversity, Biogeochemistry, 114, 93–120, https://doi.org/10.1007/s10533-012-9803-3, 2013.

565 Qian, L., Yu, X., Gu, H., Liu, F., Fan, Y., Wang, C., He, Q., Tian, Y., Peng, Y., Shu, L., Wang, S., Huang, Z., Yan, Q., He, J., Liu, G., Tu, Q., and He, Z.: Vertically stratified methane, nitrogen and sulphur cycling and coupling mechanisms in mangrove sediment microbiomes, Microbiome, 11, 71, https://doi.org/10.1186/s40168-023-01501-5, 2023.

Qiu, D., Zhong, Y., Chen, Y., Tan, Y., Song, X., and Huang, L.: Short-Term Phytoplankton Dynamics During Typhoon Season in and Near the Pearl River Estuary, South China Sea, J. Geophys. Res. Biogeosciences, 124, 274–292,
570 https://doi.org/10.1029/2018JG004672, 2019a.

Qiu, D., Zhong, Y., Chen, Y., Tan, Y., Song, X., and Huang, L.: Short-Term Phytoplankton Dynamics During Typhoon Season in and Near the Pearl River Estuary, South China Sea, J. Geophys. Res. Biogeosciences, 124, 274–292, https://doi.org/10.1029/2018JG004672, 2019b.

Qiu, H., Liu, D.-T., Wu, Y.-Z., Li, S.-Y., Ding, S., Hu, K., Zhang, J., and Chen, M.-T.: [Investigating the Pollutants of Marine
575 Shipping Emissions Along the East China Sea by Combining in-situ Measurements and Automatic Identification System], Huan Jing Ke Xue Huanjing Kexue, 43, 4338–4347, https://doi.org/10.13227/j.hjkx.202110069, 2022.

Rani, V., Schwing, P. T., Jayachandran, P. R., Preethy, C. M., Sreelekshmi, S., Joseph, P., and Bijoy Nandan, S.: Carbon stocks and sequestration rate in mangroves and its major influencing factors from highly urbanised port city, southern India, J. Environ. Manage., 335, 117542, https://doi.org/10.1016/j.jenvman.2023.117542, 2023.

580 Rong, L. I. and Rui-Ying, C.: Effects of external nitrogen additions on soil organic carbon dynamics and the mechanism, Chin. J. Plant Ecol., 39, 1012, https://doi.org/10.17521/cjpe.2015.0098, 2015.

Sasmito, S. D., Kuzyakov, Y., Lubis, A. A., Murdiyarso, D., Hutley, L. B., Bachri, S., Friess, D. A., Martius, C., and Borchard, N.: Organic carbon burial and sources in soils of coastal mudflat and mangrove ecosystems, CATENA, 187, 104414, https://doi.org/10.1016/j.catena.2019.104414, 2020.

585 Su, S., Zeng, Y., Zhao, D., Zheng, Z., and Wu, X.: Optimization of net primary productivity estimation model for terrestrial vegetation in China based on CERN data, Acta Ecol. Sin., 42, 1276–1289, https://doi.org/10.5846/stxb202011263031, 2021.

Tang, Z., Wang, D., Tian, X., Bi, X., Zhou, Z., Luo, F., Ning, R., and Li, J.: Exploring the factors influencing the carbon sink function of coastal wetlands in the Yellow River Delta, Sci. Rep., 14, 28938, https://doi.org/10.1038/s41598-024-80186-8, 2024.

590 U.S. EPA: CMAQ Model Version 5.3 Input Data: 1/1/2016–12/31/2016 12 km CONUS [Data set], 2019.

Wang, F., Chen, N., Yan, J., Lin, J., Guo, W., Cheng, P., Liu, Q., Huang, B., and Tian, Y.: Major Processes Shaping Mangroves as Inorganic Nitrogen Sources or Sinks: Insights From a Multidisciplinary Study, J. Geophys. Res. Biogeosciences, 124, 1194–1208, https://doi.org/10.1029/2018JG004875, 2019.

Wang, Q., Han, G., and Zhang, Q.: China promotes coastal wetland restoration to protect wetland ecosystems, Environ. Sci.
595 Eur., 37, https://doi.org/10.1186/s12302-025-01086-w, 2025.

Wang, Y., Yang, M., Pan, Y., Zhu, W., Long, Z., Liu, X., and Gu, X.: Valuation of the organic matter produced by terrestrial vegetation ecosystems in China in 1995 based on remote sensin, Ecol. Environ., 14, 455–459, 2005.

Wu, Y., Blodau, C., Moore, T. R., Bubier, J., Juutinen, S., and Larmola, T.: Effects of experimental nitrogen deposition on peatland carbon pools and fluxes: a modelling analysis, Biogeosciences, 12, 79–101, https://doi.org/10.5194/bg-12-79-2015, 2015.

Xia, S., Wang, W., Song, Z., Kuzyakov, Y., Guo, L., Van Zwieten, L., Li, Q., Hartley, I. P., Yang, Y., Wang, Y., Andrew Quine, T., Liu, C., and Wang, H.: Spartina alterniflora invasion controls organic carbon stocks in coastal marsh and mangrove soils across tropics and subtropics, Glob. Change Biol., 27, 1627–1644, https://doi.org/10.1111/gcb.15516, 2021.

Xiu, A. and Pleim, J. E.: Development of a Land Surface Model. Part I: Application in a Mesoscale Meteorological Model., J. Appl. Meteorol., 40, 192–209, https://doi.org/10.1175/1520-0450(2001)040<0192:DOALSM>2.0.CO;2, 2001.

Xu, L., Pye, H. O. T., He, J., Chen, Y., Murphy, B. N., and Ng, N. L.: Experimental and model estimates of the contributions from biogenic monoterpenes and sesquiterpenes to secondary organic aerosol in the southeastern United States, Atmospheric Chem. Phys., 18, 12613–12637, https://doi.org/10.5194/acp-18-12613-2018, 2018a.

Xu, W., Zhao, Y., Liu, X., Dore, A. J., Zhang, L., Liu, L., and Cheng, M.: Atmospheric nitrogen deposition in the Yangtze River basin: Spatial pattern and source attribution, Environ. Pollut., 232, 546–555, https://doi.org/10.1016/j.envpol.2017.09.086, 2018b.

Yoshikai, M., Nakamura, T., Suwa, R., Rollon, R., and Nadaoka, K.: Measurement and Modeling of Above-Ground Root Systems as Attributes of Flow and Wave Attenuation Function of Mangroves, in: Mangroves: Ecology, Biodiversity and Management, edited by: Rastogi, R. P., Phulwaria, M., and Gupta, D. K., Springer, Singapore, 279–303, https://doi.org/10.1007/978-981-16-2494-0_12, 2021.

Yuan, Y., Zhang, Y., Mao, J., Yu, G., Xu, K., Zhao, J., Qian, H., Wu, L., Yang, X., Chen, Y., and Ma, W.: Diverse changes in shipping emissions around the Western Pacific ports under the coeffect of the epidemic and fuel oil policy, Sci. Total Environ., 879, 162892, https://doi.org/10.1016/j.scitotenv.2023.162892, 2023.

Zhang, X., Liu, L., Zhao, T., Wang, J., Liu, W., and Chen, X.: Global annual wetland dataset at 30 m with a fine classification system from 2000 to 2022, Sci. Data, 11, 310, https://doi.org/10.1038/s41597-024-03143-0, 2024.

Zhao, Y., Zhang, L., Pan, Y., Wang, Y., Paulot, F., and Henze, D. K.: Atmospheric nitrogen deposition to the northwestern Pacific: seasonal variation and source attribution, Atmospheric Chem. Phys., 15, 10905–10924, https://doi.org/10.5194/acp-15-10905-2015, 2015.

Zheng, B., Tong, D., Li, M., Liu, F., Hong, C., Geng, G., Li, H., Li, X., Peng, L., Qi, J., Yan, L., Zhang, Y., Zhao, H., Zheng, Y., He, K., and Zhang, Q.: Trends in China's anthropogenic emissions since 2010 as the consequence of clean air actions, Atmospheric Chem. Phys., 18, 14095–14111, https://doi.org/10.5194/acp-18-14095-2018, 2018.

Zheng, L. and Zhai, W.: Excess nitrogen in the Bohai and Yellow seas, China: Distribution, trends, and source apportionment, Sci. Total Environ., 794, 148702, https://doi.org/10.1016/j.scitotenv.2021.148702, 2021.

Zhu, W., Pan, Y., He, H., Yu, D., and Hu, H.: Simulation of maximum light use efficiency for some typical vegetation types in China, Chin. Sci. Bull., 51, 457–463, https://doi.org/10.1007/s11434-006-0457-1, 2006.